*Journal of Archaeological Science* (2001) **28,** 643–659
doi:10.1006/jasc.2000.0634, available online at http://www.idealibrary.com on IDEAL®

# Bone Preservation in Hayonim Cave (Israel): a Macroscopic and Mineralogical Study

Mary C. Stiner*, Steven L. Kuhn and Todd A. Surovell

*Department of Anthropology, Building 30, University of Arizona, Tucson, AZ 85721-0030, U.S.A.*

Paul Goldberg

*Department of Archaeology, Boston University, 675 Commonwealth Avenue, Boston, MA 02215, U.S.A.*

Liliane Meignen

*URA 28, CEPAM-CNRS, 250 rue Albert Einstein, Sophia Antipolis 06565 Valbonne, France*

Stephen Weiner

*Structural Biology Department, Weizmann Institute of Science, 76100 Rehovot, Israel*

Ofer Bar-Yosef

*Department of Anthropology, Peabody Museum, Harvard University, Cambridge, MA 02138, U.S.A.*

(*Received 23 May 2000; revised manuscript accepted 12 October 2000*)

Understanding the cause of patchy bone distributions in archaeological sites requires that one distinguish bone decomposition in place from ''empty'' areas where bones were never present. Marked horizontal variations in bone abundance are found in the thick Mousterian layer (E) of Hayonim Cave, a large Paleolithic site in northern Israel. Infra-red analyses of minerals in the sediments identify zones of advanced diagenesis and decomposition alongside zones whose chemistry clearly favoured the preservation of bones and wood ash. These differences adhere closely to the distribution of recognizable bones in the deposits, indicating that spatial variation in bone abundance is essentially a product of differential preservation conditions. However, the few bones present in the bone-poor units are in surprisingly good condition. The higher degree of abrasion damage and more random orientations of these bones indicate that small amounts of recent material were introduced into older layers by small burrowing animals and perhaps localized trampling. The ratio of post-Mousterian to Mousterian artifacts in layer E, and the numeric contrasts in bone abundance among stratigraphic units, indicate that time-averaging from mechanical intrusion was quantitatively unimportant (2–5%) throughout this>2·4 m thick layer. Our findings support Karkanas *et al*. (2000) suggestion that bone and ash mineral diagenesis in caves follow step-wise rather than gradual transformations in geological time. Good preservation environments can be distinguished from poorer ones on the basis of mineral assemblages in sediments, and deposits that once contained bone and wood ash can be identified long after the visible traces of these materials have disappeared.


*Keywords:* PALEOLITHIC, HAYONIM CAVE, LEVANT, CARBONATE AND PHOSPHATE DIAGENESIS, VERTEBRATE TAPHONOMY, BONE PRESERVATION, INFRA-RED SPECTROSCOPY.

## Introduction

Two materials common to some archaeological sites, animal bone and wood ash, are rich in phosphate and carbonate compounds,

*To whom correspondence should be addressed. Email: mstiner@u.arizona.edu.



0305–4403/01/060643+17 $35.00/0

respectively. Bone mineral is composed of the calcium phosphate mineral dahllite, also known as carbonated apatite (McConnell, 1952), whereas fresh wood ash contains mainly calcite. The mineral components of vertebrate skeletons, mollusc shells (mainly aragonite), ostrich eggshell (calcite) and burned wood are all susceptible to dissolution and recrystallization in a variety of acidic sedimentary conditions. Heating and fossilization promote recrystallization of bone mineral, crystals of which may grow and become more orderly post-mortem (Hedges & Millard, 1995; Shipman, Foster & Schoeninger, 1984; Stiner *et al.*, 1995). Dissolution removes minerals, which may then reprecipitate elsewhere. The processes of dissolution and recrystallization require water, a powerful and common solvent, tempered by the presence of organic compounds and the parent geochemistry of the matrix containing bones and ash (Hedges & Millard, 1995; Hedges, Milard & Pike, 1995; Karkanas *et al.*, 2000; Weiner & Bar-Yosef, 1990).

Because mineral is the major component of bone, substantial loss of mineral should reduce a bone's visibility and identifiability in sediments. Perhaps the main factor influencing bone dissolution is pH. Reduction in pH that almost inevitably occurs when organic matter is oxidized (Berner, 1971) will lead to bone dissolution, as opposed to the presence of calcite in sediments, which stabilizes pH at around 8·0 and thus minimizes dissolution This is not to say that mineral decomposition proceeds at a gradual pace—a variety of studies indicate that dissolution is promoted by subtle changes in sediment chemistry and may proceed rapidly (Hedges, Millard & Pike, 1995; Karkanas *et al.*, 2000; Weiner, Golberg & Bar-Yosef, 1993; Weiner & Bar-Yosef, 1990). However, dissolution accompanied by reprecipitation should leave characteristic decomposition traces in its wake. Wood ash contains minor, highly resistant mineral components, siliceous aggregates and phytoliths, which persist in sediments after carbonates and phosphates have been flushed from the system (Schiegl *et al.*, 1994, 1996; Albert *et al.*, 1999). The presence of calcite and/or dahllite in sediments* indicates that conditions are conducive to good preservation of bones and wood ash (Schiegl *et al.*, 1996; Weiner *et al.*, 1993). When calcite and/or dahllite are absent from the sediments, and the proportions of the resistant fraction of ash are high (Schiegl *et al.*, 1996), one may conclude that bones would not have been preserved (Weiner, Goldberg & Bar-Yosef, 1993). These points apply as well to mollusc shell, if originally part of faunal assemblages, since aragonite is even more unstable than calcite.

The fact that buried bones and wood ash can dissolve *in situ* raises the question of whether these materials were once present in archaeological excavation units that lack them today. Differential bone preservation can take the form of uneven spatial distributions in sediments or, to a lesser extent, biases in skeletal element representation relative to the complete vertebrate anatomy. We are concerned mainly with differential preservation among excavation units in this study: how dissolution may distort archaeologists' perceptions of site structure and human disposal behaviour, and what can be done to control for its effects.

Flint artifacts are ubiquitous in the Mousterian layer of Hayonim Cave, whereas bones and visible traces of fire display very uneven distributions. Distinguishing human from preservation effects in this case requires information on the sedimentary environment as well as the condition of the bones in question. We examine (1) the condition of wood ash residues and other minerals in the sediments using infra-red spectroscopy, and compare these findings to (2) infra-red data on bone mineral condition and (3) macroscopic observations of bone damage such as fragmentation, the ratio of porous to compact tissue types, and abrasion. The results of these analyses point to yet another process, (4) mechanical disturbance in the strata column, the scale of which is evaluated in part from the proportion of intrusive (post-Mousterian) artifacts. Our study applies infra-red sampling of bones and sediments on great numeric and spatial scales, and fully cross-references the results of mineralogic and macroscopic bone data sets. In addition to answering questions specific to Hayonim Cave, we isolate variables suitable for addressing site formation processes and faunal preservation in general, and for Mediterranean caves in particular.

## Archaeological Background

Hayonim Cave lies in the western Galilee of Israel (Figure 1(a)). Its long history of human occupation began more than 200,000 years ago and continued into the historic period. Artifacts and faunal remains are prevalent in the Natufian layer (B, in Figure 2), Kebaran layer (C), Levantine Aurignacian layer (D), and Mousterian or Middle Paleolithic layer (E) (Bar-Yosef, 1991; Belfer-Cohen & Bar-Yosef, 1981; Tchernov, 1994). Layer E is about 2·4 m thick in the central excavation trench, and spans tens of thousands of years of deposition. Its earliest components date to the later part of the Middle Pleistocene epoch (Tchernov, 1998; Valladas *et al.*, 1998; Schwarcz & Rink, 1998), The co-occurrence of well preserved faunal remains and early Middle Paleolithic artifacts provided incentive for renewed excavation at the site in 1992–1999 (Bar-Yosef, 1998; Goldberg & Bar-Yosef, 1998; Stiner & Tchernov, 1998).

Our study sample comes from the central excavation trench in Chamber I (Figure 1(b)), where the

*The sediments are not only the product of diagenetically altered ash and bones. In fact the phosphate comes from the organics and the aluminum, magnesium, probably from clays, and so on. We focus here on the significance of calcite and dahllite as it concerns bone preservation.

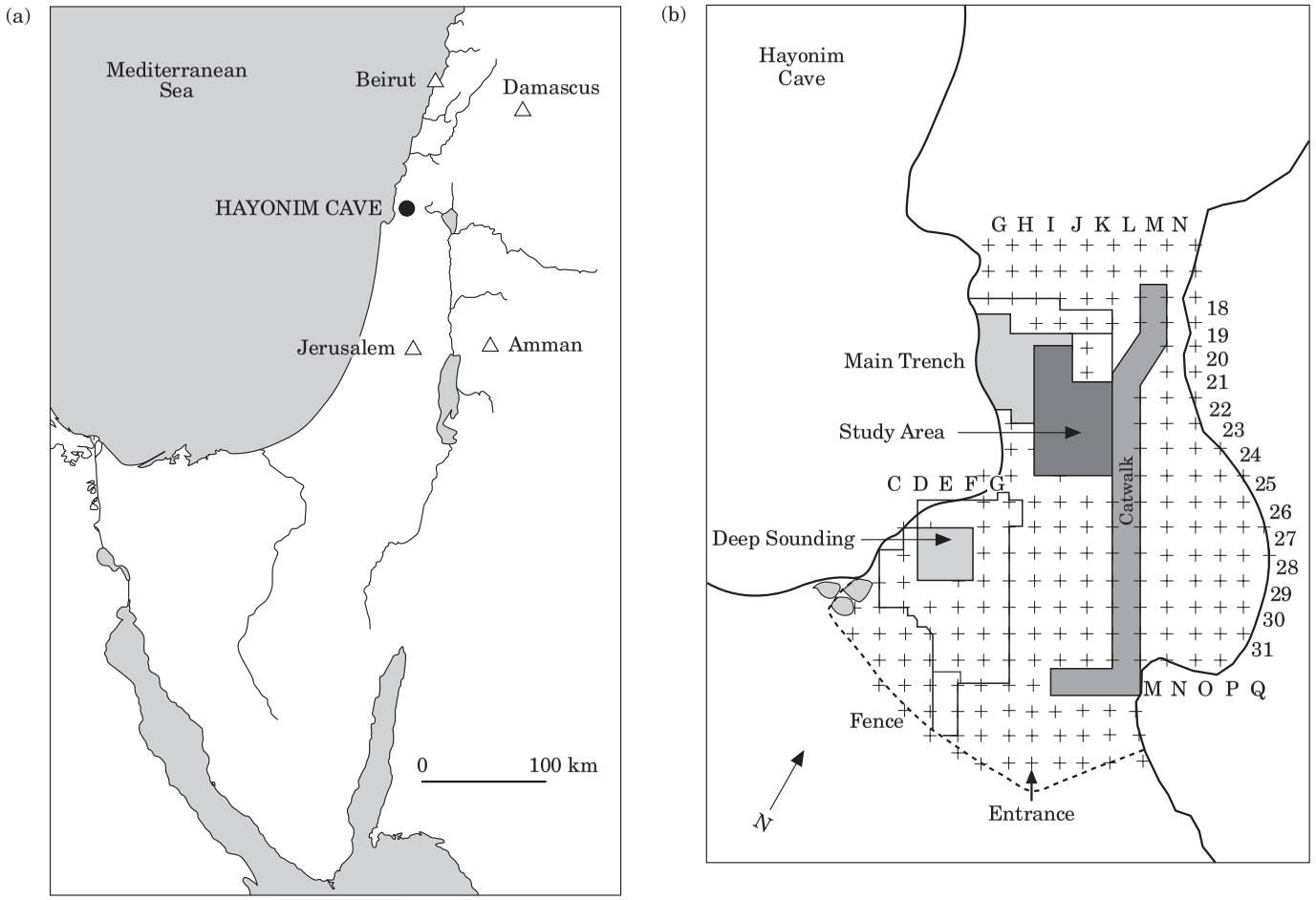


Figure 1. Location of Hayonim Cave in the Galilee of northern Israel (a), and plan view of the excavations (b). The assemblages for this study come from the deeply shaded area of the "central" trench (squares I-K, 20–24). The dashed line represents fence enclosing the entrace; the modern drip line is located just north of this line.

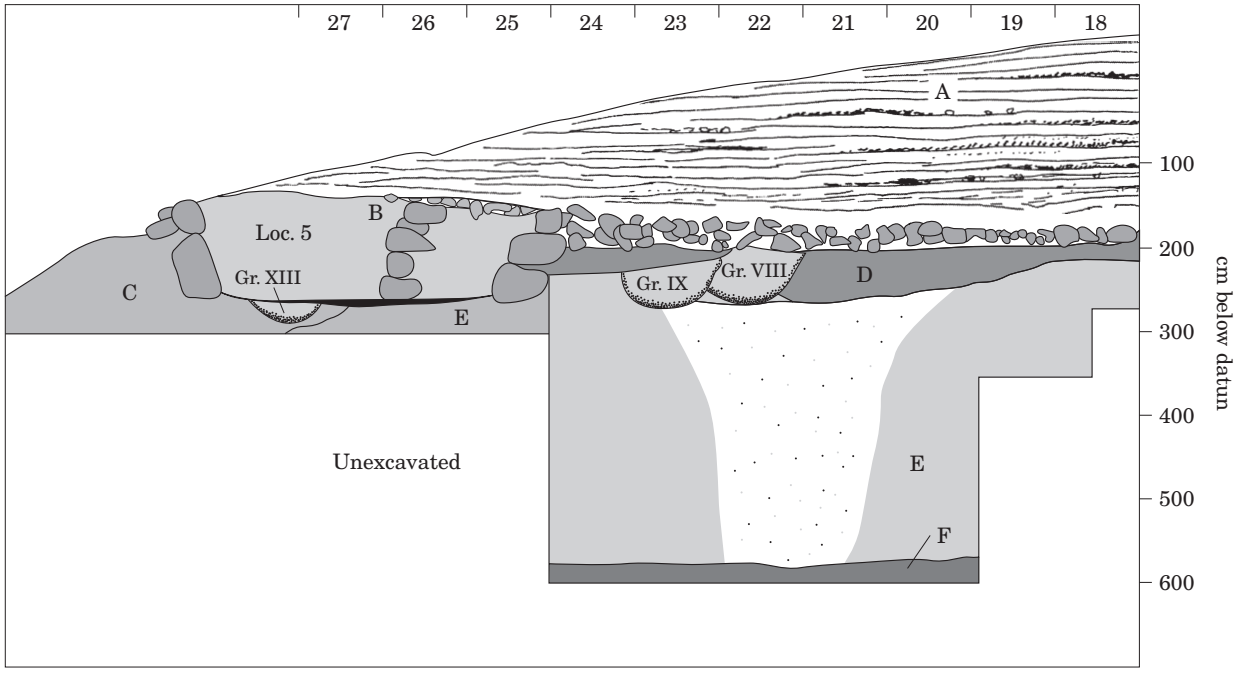


Figure 2. A north–south cross section of the central trench, showing the positions of the Levantine Aurignacian (D) and younger cultural deposits dating to the Kebaran (C) and Natufian (D), above the Mousterian layer (E); graves (Gr.) are Natufian age; the recently exposed Layer F contains little bone of any sort. The Aurignacian layer, excavated many years ago, was uniformly rich in bone, in contrast to the patchy bone distributions in the Mousterian layer below it. There is evidence of an erosional unconformity separating the Mousterian deposit and the Aurignacian, a hiatus in deposition lasting as long as 70,000 years.

Mousterian layer is overlain by younger Aurignacian and, to a lesser extent, Natufian deposits (Figure 2). Bedding in layer E is generally horizontal throughout this area (squares I-K 20-24). Animal bones and Mousterian artifacts are particularly abundant between 400 and 470 cm below datum (bd) (Figure 3); they are present in lower numbers up to about 300 cm bd, and down to about 520 cm bd. In contrast to the continuous distribution of lithic artifacts in the Mousterian layer, a diagonal swath nearly devoid of bones bisects the central trench area top-to-bottom (Figure 4). The boundaries of this peculiar feature are sharp. The bone beds are densest under calcareous breccia shelves, where seeping water eventually was shunted by flowstones and localized calcium saturation. Isolated, layered "hearth areas" rich in charcoal and recognizable ash lenses (Figure 5) are common where bones are abundant but generally absent where bones are rare.

The "bone-poor" zone does not lack bone entirely, however; bones are just conspicuously few in comparison to nearby units. Below 470 cm bd, the positions of bone-poor and "bone-rich" zones shift somewhat, but the contrasting distributions of bones and stone artifacts persist. The consistently diverse orientations of the long axes of piece-plotted stone artifacts (Figure 6) and bones (Figure 7) in the sediments indicate no alignment biases in the "bone-rich" or the "bone-poor" zones, although bone orientations are the most varied in the bone-poor units. Thus there is no evidence of hydrological sorting or removal, refuting the possibility that the bone-poor swath represents an erosional channel. Localized dissolution may account for the markedly uneven distribution of bones in Layer E. If so, it occurred before the formation of the Aurignacian layer (D), which was uniformly rich in bone. This hypothesis is tested in the next section, followed by an exploration of minor but informative contradictions to the main results.

## Two Hypotheses of Bone Assemblage Formation

Differences in bone and flint artifact distributions in Hayonim Cave are easily appreciated from the maps of piece-plotted materials. These observations raise two contrasting hypotheses and sets of test implications about bone assemblage formation in the Mousterian layer:

(1) The heterogeneous distribution of bones is the result of spatially discrete disposal behaviour by humans, evidently not practiced for stone artifacts; that is, bones never were deposited in some units but were preferentially deposited in others. If the preservation environment did not vary among units, the condition of the few faunal specimens present in the bone-poor zone should be about the same as for those occurring in the bone-rich zone. The sediments in bone-poor units should contain plentiful calcite or dahllite.

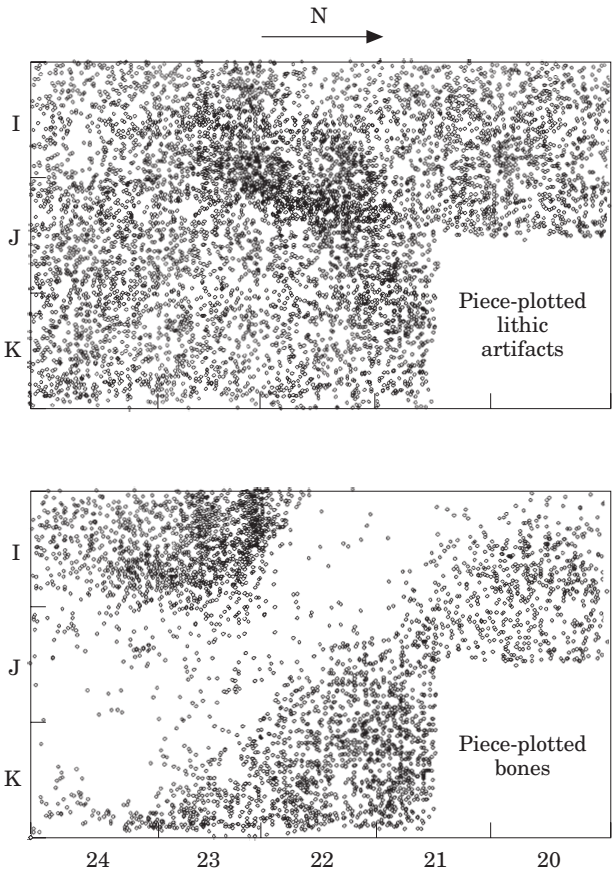


Figure 3. Comparison of the spatial distributions of piece-plotted lithics (top) and bones (bottom) in the Mousterian layer between 300 and 540 cm bd of the central trench, viewed from above. Horizontal spatial units are metres. The mild clustering apparent in the lithics distribution is due only to a small concentration of artifacts encountered at the boundary of layers E and F.

Figure 5. Mousterian hearth lenses exposed in the north wall (west of travertine deposits) of central excavation trench.

(2) The heterogeneous distribution of bones is the result of differential preservation over a scale of metres. Whatever caused the near disappearance of bones in the central, bone-poor zone operated almost exclusively in this spatial domain for tens of thousands of years. Bones were once present in all units, but were dissolved locally in some units and preserved in others. The few specimens in the bone-poor zone should be in semi-altered states as remnants of a nearly completed dissolution process. Sediments of bone-poor units should not contain much dahllite and calcite, but should retain the more stable decomposition products of these parent minerals.

## Infra-red and Macroscopic Methods

Two distinct analytical scales are employed to evaluate the hypotheses. The first is molecular and, using Fourier-Transform Infra-red (FTIR) spectroscopy,

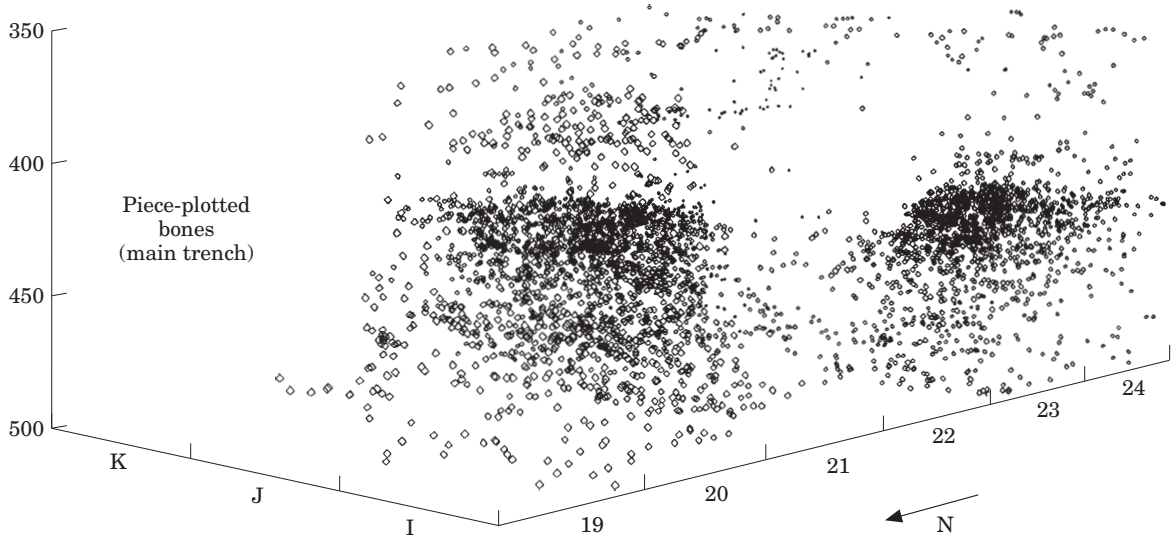


Figure 4. Three-dimensional view of the distribution of piece-plotted bones from the Mousterian layer (E) of the central trench. Horizontal spatial units are metres; vertical increments are cm.

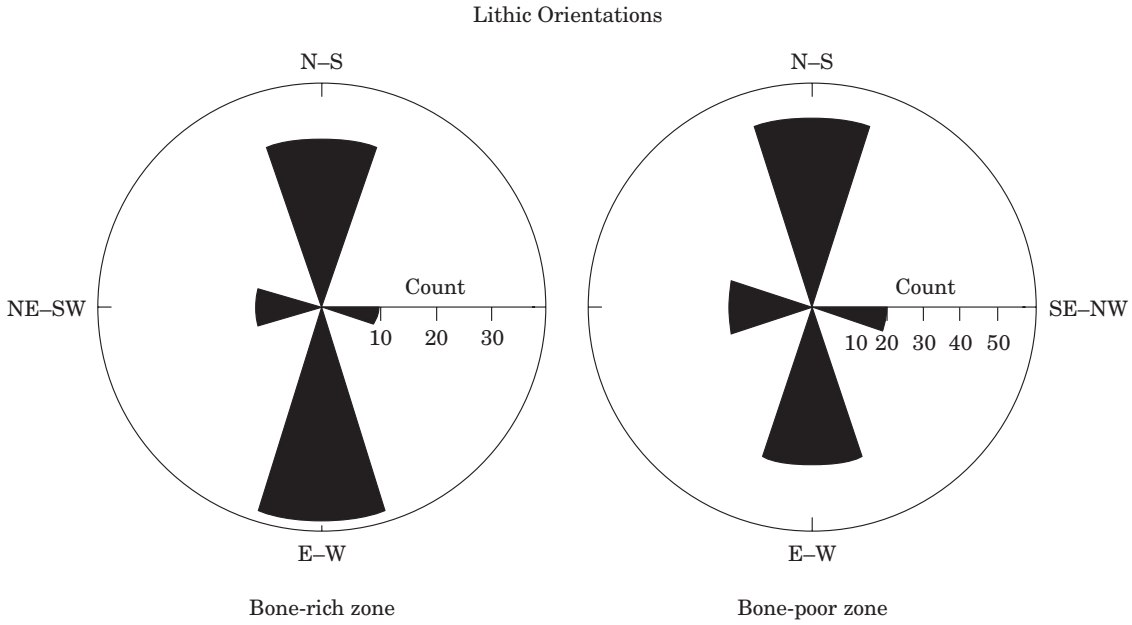


Figure 6. Orientations of piece-plotted lithic artifacts in the (a) bone-rich and (b) bone-poor zones of the central trench. Frequency distributions are shown according to four potential axes: N–S, E–W, NE–SW and SE–NW.

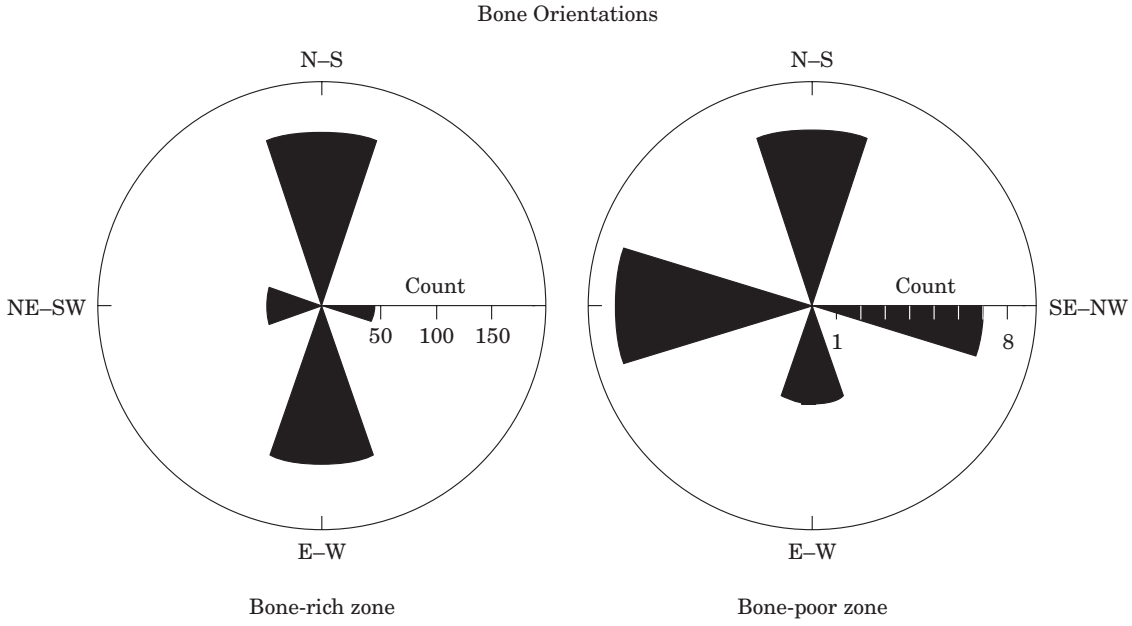


Figure 7. Orientations of piece-plotted bones in the (a) bone-rich and (b) bone-poor zones of the central trench. Frequency distributions are shown according to four potential axes: N–S, E–W, NE–SW, and SE–NW.

focuses on the condition of biologically generated minerals in relation to independently established diagenetic sequences. While the state of bone mineral preservation is the primary issue here, these results are compared to FTIR data from the surrounding sediments (Weiner *et al.*, in preparation). FTIR analysis is well suited to research on carbonate and phosphate compounds, including their reconstitution and decay (Weiner *et al.*, 1995), because it reflects the strength and arrangements of molecular bonds and the relative orderliness of crystal structure (Smith, 1996).

Abundant calcite and dahllite in sediments indicate good preservation conditions for bones and ash because these minerals are relatively unstable and dissolve easily. Extensive diagenesis is indicated instead by the prevalence of decomposition products and an abundance of resistant silica components in sediments (Schiegl *et al.*, 1996; Karkanas *et al.*, 1999). We examine sediment con-

tent and bone condition in relation to bone abundance by weight across multiple spatial units in the central trench. We also seek evidence of bone diagenesis independent of the spatial distributions of bone using differences in specimen surface area, as measured coarsely by gross length and tissue class (spongy, compact and stony) to assess the extent of *in situ* alterations of bone.

The second analytical scale is macroscopic and focuses on variation in bone damage characteristics such as fragment length (cm), burning, and abrasion, in conjunction with skeletal tissue type, bone abundance per excavation unit ($50 \times 50 \times 5$ cm), and specimen identifiability. Mechanical and chemical decomposition should have consequences for most or all of these damage characteristics. Quantitative units for the analyses are number of specimens (NSP), number of identified specimens (NISP), number of unidentifiable specimens (NUSP), and total bone weight (g) per $50 \times 50 \times 5$ cm excavation unit.

### *Infra-red spectroscopy of bones and sediments*

Dissolution removes mineral from bone, just as it removes carbonates and phosphates from surrounding sediments. Recrystallization involves molecular reorganization of the bone's mineral component but is not necessarily independent of dissolution (Hedges, Millard & Pike, 1995). While these diagenetic processes can be induced by many factors, water and neutral-to-low pH are essential for dissolution and recrystallization (Karkanas *et al.*, 2000; Schiegl *et al.*, 1994; Shipman, Foster & Schoeninger, 1984; Stiner *et al.*, 1995; Weiner & Bar-Yosef, 1990; Weiner, Goldberg & Bar-Yosef, 1993; Ziv & Weiner, 1994).

Bone mineral recrystallization can be measured more or less directly using the infra-red index known as the splitting factor (SF) (Termine & Posner, 1966). Probable loci of high dissolution can be identified from decline in the sediments of the two unstable minerals most beneficial to preservation—dahllite and calcite (Weiner & Goldberg, 1990; Weiner, Goldberg & Bar-Yosef, 1993). Phosphate in cave sediments may originate from biological sources (e.g., guano, organic refuse) or as decomposition by-products of fresh wood ash or limestone bedrock. Our method does not distinguish primary and secondary sources of phosphates—it only recognizes their presence or absence in the form of phosphate-containing minerals. Regardless of origin, calcite and dahllite in sediments is consistent with bone preservation, a relation well demonstrated in Kebara Cave, Israel (Weiner, Goldberg & Bar-Yosef, 1993). Decomposition of calcite and dahllite may follow one of several pathways, leaving products as diverse as taranikite, montgomeryite, leucophosphite, and variscite, among others (Karkanas *et al.*, 1999; Schiegl *et al.*, 1996); in addition siliceous aggregates may derive from wood ash (Schiegl *et al.*, 1994).

More than 1400 sediment samples and over 600 bone samples were subjected to infra-red spectroscopy, using two Midac Corporation (Costa Mesa, U.S.A.) Fourier-transform infra-red (FTIR) spectrometres, operated by Spectracalc (for Ms-Dos) or Grams 386 (for Windows 95) software (Galactic Industries Corp., Salem, New Hampshire, U.S.A.). Sediment samples were obtained throughout Layer E and analysed on site. Nearly all of these sediments contain ash derivatives of some kind, albeit in varied concentrations and states of preservation (Weiner *et al.*, in prep.). FTIR sample preparation for sediment samples is straightforward, as the matrix is examined only for rank-order abundance of key minerals, most importantly carbonates, phosphates, quartz, clay, manganese, and silica compounds. Each sediment sample was ground in an agate mortar and pestle. An extract of a few micrograms of this was mixed with a few tens of milligrams of KBr powder, ground again, pressed into a 7 mm diameter pellet using a Quik Handipress (following Weiner, Goldberg & Bar-Yosef, 1993), and then inserted into the sample chamber of the infra-red spectrometer.

The FTIR analyses of bone were done at the University of Arizona (Tucson), U.S.A., owing to the emphasis on quantitative variation in bone spectra and the more elaborate system needed to standardize the pellet preparation procedure and control analyst-induced error; experimentally based refinements in pellet production effectively keep SF measurement error to no more than $\pm 0{\cdot}05$ (for a complete technical description, see Surovell & Stiner, 2001). Altered bone may be mineralogically heterogeneous, necessitating the use of relatively large, apparently homogeneous bone samples. After mechanically cleaning the surface of a specimen, a piece approximately 10 mm in diameter and at least 3–5 mm thick was homogenized by pulverization for 15 seconds in a Wig-L-Bug ball mill, using a steel capsule and mortar ball. This powder was sifted through nested 45 and 63 μm mesh screens to limit the particle size range. The powder fraction collected within this size range was added to powdered KBr at a ratio of 1% bone to 99% KBr. The mixture was returned to the Wig-L-Bug mill for an additional 30 sec of regrinding and blending. A 50 mg extract of the fully homogenized mixture was then pressed into a pellet in the manner described above.

The FTIR analysis of bone uses four infra-red peak indexes: the dahllite crystallinity index called splitting factor (SF);‡ and the carbonate ($876\ cm^{-1}$), water ($3500\ cm^{-1}$), and calcite ($712\ cm^{-1}$) peaks, each

‡An expanded infra-red spectrum in the 425–900 $cm^{-1}$ range is used to measure SF, based on the method of Weiner & Bar-Yosef (1990). The ratios of the absorption band of carbonate at 874 $cm^{-1}$ to the 565 $cm^{-1}$ phosphate peak are used to semi-quantitatively estimate relative carbonate contents of the mineral phase. This follows Featherstone, Pearson & LeGeros (1984), who, by using synthetic standards, showed that the ratio of the carbonate 1415 $cm^{-1}$ absorption band to the same phosphate band reliably estimates ($\pm 10\%$) carbonate content. We used the 874 $cm^{-1}$ carbonate adsorption rather than the 1415 $cm^{-1}$ adsorption, because the latter was affected by the presence of organic matrix absorption bands in the relatively well-preserved bones.

standardized to the 563 $cm^{-1}$ phosphate peak. Although not a direct measure of dissolution, SF is useful for tracking diagenesis in general since low temperature recrystallization also requires water. The extent of splitting of the two absorptions at 603 and 565 $cm^{-1}$ reflects a combination of the relative sizes of the crystals in bone mineral and the orderliness of the atoms in the crystal lattice (Termine & Posner, 1966). As recrystallization progresses, the two absorption peaks become increasingly separate, measured as the average of the heights of the two peaks (baseline drawn between 495–750 $cm^{-1}$) divided by the height of the low point between them (Weiner & Bar-Yosef, 1990: 189–190). The higher the SF value, the larger and/or more ordered are the crystals. SF is always lowest for fresh bone (about 2·5–2·9), because the dahllite crystals are small when formed in living bone (Robinson, 1952; Weiner & Price, 1986). SF may increase post-mortem to 4·5–5·0 (and exceptionally to as much as 7·0) under ambient temperatures, as large crystals grow at the expense of small ones. SF is highest for bone heated to a calcined state (7·0+). As SF increases with heating, carbonate decreases (e.g., Person *et al.*, 1996; Stiner *et al.*, 1995: Figure 4) because the original dahllite lattice recrystallizes and, in so doing, loses carbonate to form hydroxyapatite. Splitting factor thus is an index of crystallinity. The simpler SF measurement of Weiner and Bar-Yosef (1990) is very strongly correlated to Termine and Posner's (1966) measure in our data set ($r$=0·93, $P$<0·0001) and thus is assumed to measure the same thing.

Recrystallization of buried bone may occur gradually over many years, as part of fossilization, or through rapid transformations caused by weathering over a few months to decades (Stiner *et al.*, 1995). By contrast, high temperature diagenesis is nearly instantaneous, especially above 650°C, when solid state recrystallization occurs (Shipman, Foster & Schoeninger, 1984; Stiner *et al.*, 1995). Much of the bone diagenesis in the Mousterian layer of Hayonim Cave occurred at ambient or low burning temperatures, exceptions being those few bones calcined by fire. Because we want to know about ambient temperature recrystallization of bone mineral, burned and obviously weathered bones were excluded from the FTIR analysis based on visual inspection; darkened specimens of any sort were avoided. The FTIR bone sample is primarily from a SW–NE transect of the central trench, oriented to cross-cut maximum variation in bone abundance (Figure 8). Bones in the FTIR sample set were also examined for macroscopic damage characteristics.

*Macroscopic analyses of bone*

The macroscopic study of bone damage includes 15,492 identifiable skeletal specimens (NISP) recovered throughout the central trench between 300 to 540 cm bd in Layer E. The great majority of these specimens

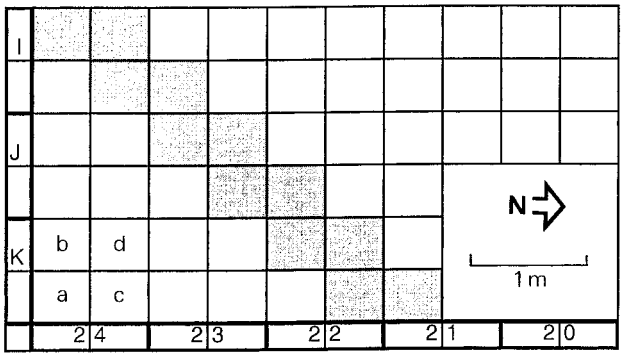


Figure 8. Transect placement in the central trench. There are twelve 50 × 50 × 5 cm units over a depth of 1·2 m, oriented to cross-cut maximum variation in bone abundance.

are fragmented. In addition, 3768 unidentifiable specimens (NUSP) from the transect area (see Figure 8) were examined. The FTIR bone samples (>600) are also unidentifiable fragments, raising the total NUSP from the transect to >4400, although the macroscopic qualities of the FTIR set are analysed separately. The macroscopic variables considered here are (1) maximum fragment length in cm; (2) presence of burning damage; (3) identifiability to element and taxon or body size class (otherwise considered "unidentifiable"); (4) tissue macrostructure ranging from spongy to compact to "stony" enamel (following Wainwright *et al.*, 1976); and (5) presence and intensity of abrasion damage.

## Sediment Mineralogy versus Bone Abundance

Prior work in Hayonim and Kebara caves (Weiner, Goldberg & Bar-Yosef, 1993; Schiegl *et al.*, 1996) identified diagenetic sequences that remove calcite and dahllite and leave behind montgomeryite, leucophosphite, variscite, and siliceous aggregates in the sediments. Some of the chemical pathways observed in these two sites may be unique to the geology of the region (compare, for example, Karkanas *et al.*, 1999). The most important distinction, however, is one common to many caves—the opposing presence of calcite and/or dahllite in sediments and that of decomposition products known to derive from these parent minerals under reactive conditions. Figures 9(a) and 10(a) show selected 10 cm thick cuts in which sediments of the bone-poor swath lack calcite or dahllite, but highly decomposed mineral phases are abundant. However, calcite and dahllite are well preserved on either side of this diagonal feature. Bone abundance by bulk weight (g), shown in Figures 9(b) and 10(b), clearly agrees with the distribution of intact dahllite and calcite in the sediments, as does the distribution of terrestrial snail shells. FTIR analysis of 38 specimens confirms that all unburned snail shells are composed of aragonite, a particularly fragile carbonate, also indicating favourable preservation conditions.

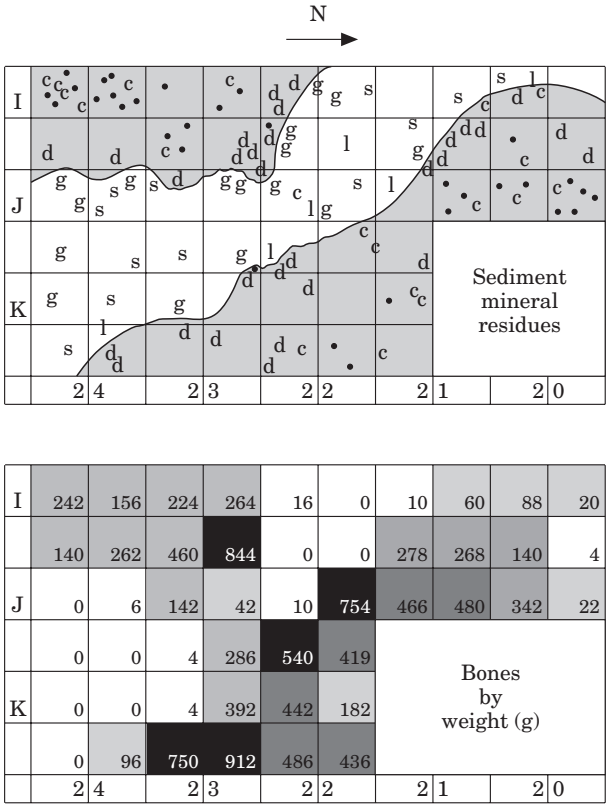


440–449 cm bd

Figure 9. The distribution of dominant minerals in sediments relative to screen-recovered bone (by weight in g) between 440 and 449 cm bd in the Mousterian layer of the central trench. Stippled shading indicates sediments containing as the major components calcite in upper frame (c) and dahllite (d)—good preservation conditions for faunal remains. Poorly preserved wood ash and/or bone residues are indicated by the presence of montgomeryite (g), leucophosphite (l), and siliceous aggregates (s) as the major components—poor preservation conditions for faunal remains. Solid dots represent preserved land snail shells. Dissolution fronts appear as solid lines. Mapping of the front was performed interactively on-site, leading to some clustering of samples on and around the dissolution boundaries. *N* sediment samples=84. (Data on bone weights are missing for three subsquares lower frame).

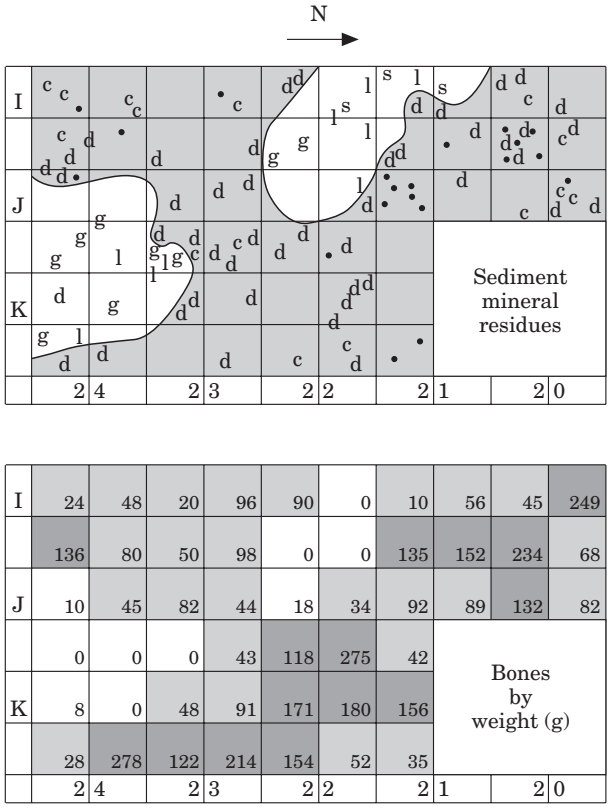


460–469 cm bd

Figure 10. The distribution of dominant minerals in sediments relative to screen-recovered bone (by weight in g) between 460 and 469 cm bd in the Mousterian layer of the central trench. Stippled shading in upper frame indicates sediments containing as the major components calcite (c) and dahllite (d)—good preservation conditions for faunal remains. Poorly preserved wood ash and/or bone residues are indicated by the presence of montgomeryite (g), leucophosphite (l), and siliceous aggregates (s) as the major components—poor preservation conditions for faunal remains. Solid dots represent preserved land snail shells. Dissolution fronts appear as solid lines. Mapping of the front was performed interactively on-site, leading to some clustering of samples on and around the dissolution boundaries. *N* sediment samples=83.

Figure 11 compares the percentage of sediment samples dominated by each of six key minerals relative to bone abundance for all units from 300 to 470 cm bd. There is a significant positive spatial relation between the mineral compositions normally conducive to ash and bone preservation and the observed quantities of bone (Spearman's $r=0{\cdot}54$, $N=521$, $P<0{\cdot}001$), in spite of the fact that point-plotted sediment results are compared to bone NISP by $50 \times 50 \times 5$ cm excavation unit. Calcite is the first compound to decline with bone abundance, followed by dahllite. The other minerals in the diagenetic cascade, representing conditions unfavourable to bone and ash preservation, predominate where bones are least abundant.

The uneven distribution of two anthropogenic materials in the central trench—faunal remains and wood ash—therefore is best explained by geochemical dissolution, not selective deposition by Middle Paleolithic humans. Dissolution did not affect the flint artifacts, the chemical composition (mainly microcrystalline $SiO_2$) of which is quite resistant to common acids.

### *Bone preservation quality: mineral condition versus specimen surface area*

Diagenetic processes involving water must be mediated in part by specimen surface area. The key question, however, is at what scale this is operative. The macroscopic surface area of any skeletal specimen increases with fragmentation while the density of the constituent fragments remains constant. Susceptibility to diagenesis therefore may increase with fragmentation.

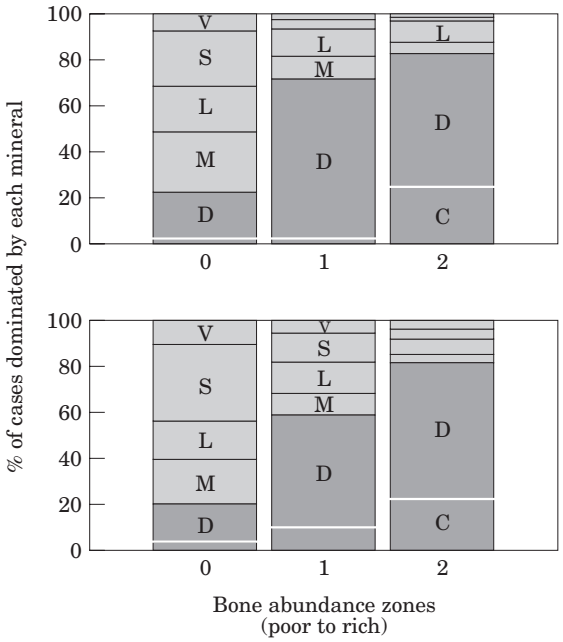


Figure 11. Percent of the total number of sediment samples dominated by each of the following minerals, organized according to bone abundance by weight (bone-poor zone=0, intermediate zone=1, bone-rich zone=2). (V) variscite, (S) siliceous aggregates, (L) leucophosphite, (M) montgomeryite, (D) dahllite, (C) calcite. Darker shading indicates relatively unaltered carbonates and phosphates, lighter shading the consecutive stages of diagenetic alteration of the parent minerals, from bad to worse.

Here bone specimen length serves as a proxy (and decidedly imperfect) measure of surface area, since nearly all of the bones are fragmented to some degree. This analysis applies mainly to the excavation units rich in bone and qualifies our perceptions of preservation quality. Specifically, we expect a negative relation between fragment length and SF, a measure of bone mineral crystallinity if diagenesis occurred. The FTIR bone data weakly fit the expectation ($r = -0{\cdot}27$, $P = 0{\cdot}0001$). This means some diagenesis occurred to the well-preserved bones, at least in the form of recrystallization, but its effects were limited.

Another way of testing for diagenetic effects at a finer scale is to compare mean SF values for two distinct bone tissue structures, spongy (cancellous) and compact types.[§] Spongy bone fragments have somewhat greater surface areas relative to volume than do compact bone fragments, although even the latter are riddled with canaliculi. Table 1 shows that SF is only slightly higher for spongy bone fragments, given a potential range of 2·8–4·5; other FTIR indexes remain constant between the two bone tissue classes. We conclude from these observations that water-mediated diagenesis affects bone crystallinity at a scale much finer than that of the visible macrostructure. As the crystals themselves have sub-micron dimensions (Robinson, 1952; Weiner & Price, 1986), this might be the critical scale for these effects: water interacts at the level of molecules or nanometers when it affects the bone mineral crystals.

Slightly higher mean SF values for smaller specimens in general, and for spongy bone specimens in particular, indicate that the surviving bones from the central trench were indeed exposed to diagenesis—at least low temperature recrystallization. While dissolution can not be measured directly by our techniques, bone crystal changes relative to exposed surface area of specimens indicate that mild water-mediated diagenesis occurred. The macroscopic condition of specimens nonetheless appears to be very good overall (Figure 12). How these observations translate to differential body part preservation in Hayonim Cave, a common concern for research on human economic behaviour, is beyond the scope of this study.

## Bone Condition versus Bone Abundance

Sediment mineralogy provides clear evidence for bone dissolution in a restricted area of the central trench, yet very good preservation elsewhere. These findings beg information about the condition of the few bone specimens present in the areas where preservation

§Mature tooth enamel represents the most resistant material (>95% mineral, Wainwright *et al.*, 1976), although it is fortified by compact dentine (approximately 70% mineral). Compact bone represents the intermediate condition because it is dense, and spongy bone is widely considered to be the least resistant to diagenesis due to its open, porous texture and higher surface area; both are 70% mineral and porous on a finer structural scale, however. The relative pace of disintegration for spongy versus compact bone and tooth enamel remains to be established.

*Table 1. SF and other FTIR index means for compact versus spongy bone specimens*†

| Bone tissue type (N obs) | SF* | | CARB:PHOS | | CALC:PHOS | | WATER:PHOS | |
|---|---|---|---|---|---|---|---|---|
| | Mean | S.D. | Mean | S.D. | Mean | S.D. | Mean | S.D. |
| compact (479) | 3·2 | 0·2 | 0·2 | 0·1 | 0·01 | 0·02 | 0·64 | 0·14 |
| spongy (75) | 3·4 | 0·3 | 0·2 | 0·1 | 0·02 | 0·04 | 0·61 | 0·12 |

†Compact bone is dense and thick-walled. Spongy bone is equally dense at the microscopic level, but thin-walled at the level of macrostructure, and possesses a higher surface area to mass once the thin cortical covering is breached. Spongy bone therefore is more vulnerable to diagenetic effects.
*The potential SF range of variation for recrystallization at low temperatures is roughly 2·8 to 4·5.
(N obs) number of faunal specimens observed.

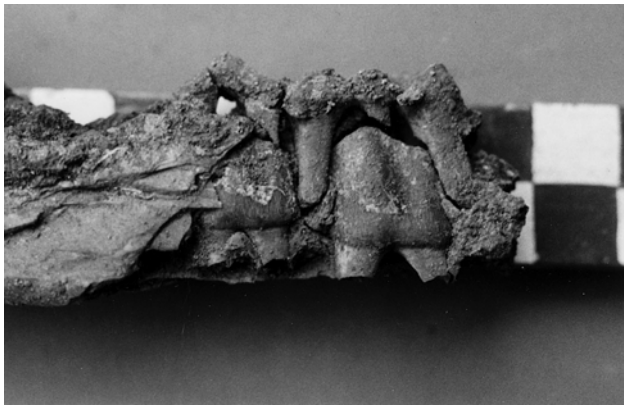

Figure 12. Representative example of the high quality of preservation observed for faunal specimens in the bone-rich excavation units.

should be poor. Here we look for indications of bone diagenesis in relation to bone distributions in space. The FTIR analysis of bone fragments is confined to the transect in the central trench (Figure 8) over a vertical range of 420 to 540 cm.

Figure 13 compares mean SF values for bones from transect unit pairs running N–S and E–W, above and below 470 cm bd (data in Table 2). Little variation exists in bone mineral crystallinity in relation to bulk bone abundance ($F$ ratio=1·588, $N$=636, $P$=0·205, $r^2$=0·005). Oddly, mean SF is consistently lower (i.e., closer to fresh bone) where bones are least abundant and ash is most diagenetically altered. To the extent that bone mineral condition varies among excavation units, SF values are the opposite of what was expected from sediment mineralogy and bone abundance. Bones in the bone-poor zone are in better, rather than worse, condition than preservation chemistry predicts.

Mean SF declines only slightly at the lower boundary of faunal assemblages in the central trench, varying between 3·2 and 3·3 before bones disappear below about 520 cm bd. There is no evidence for gradual vertical or horizontal transitions in bone condition, an observation that supports our perception of sharply bounded "dissolution fronts". Isolated specimens elsewhere in Hayonim Cave have SF values as high as 4·8 and partly decomposed appearances, but they are very rare. SF values for bone samples within the transect never exceed 4·5.

We also examined the relations of fragment size, burning damage, and skeletal tissue representation (spongy, compact, or enamel) to spatial variation in bone abundance and sediment mineralogy. The proportion of delicate to robust skeletal structures should decline with preservation conditions. However, Table 3 shows the relative frequency of fragile (spongy) bone, compact bone, and highly resistant (stony) tooth enamel to be about the same across the bone-poor to bone-rich zones. What is more, mean specimen lengths and burning frequencies bear no consistent relation to bone abundance across the bone-poor to bone-rich zones (Table 4).

In contrast to the results on sediment mineralogy, few spatial correlations exist between the most readily visible aspects of bone specimens and bulk bone abundance. The only exception is the somewhat higher degree of abrasion on bones in units where the total quantity of bone is small (see below).

## What is the Origin of the Bones in the Bone-Poor Zone?

Figure 14 shows that the severity of mechanical abrasion on FTIR-sampled bones from the central trench, ranked by visual inspection into four classes (none to most severe) relative to total bone weight per excavation unit. The degree of abrasion is always highest for specimens from units with the lowest weights for total recovered bone. A Spearman's $r$ statistic yields a value of $-0{\cdot}38$ ($N$=451, $P$<0·001) for abrasion intensity (a specimen-specific characteristic) against total bone weight (a 50 × 50 × 5 cm excavation unit characteristic), a significant relation particularly in light of the differing sampling strategies involved. Considerable tumbling or trampling is required to produce visible abrasion damage on bone, rendering these subtle frequency differences significant. The fact that abrasion is most advanced in the bone-poor excavation units suggests that these specimens were subjected to greater mechanical disturbance. More diverse inclinations of bone specimens in the bone-poor units, shown in Table 5, lend additional support to this conclusion. While the majority of the piece-plotted specimens lie horizontally in the central trench, the proportion of non-horizontal pieces is about twice as high in areas of low to moderate quantities of bone than in areas where bone is abundant. The bone and lithic orientations discussed above (see Figure 7) tell a related story.

The most likely sources of mechanical disturbance in Hayonim Cave are human traffic and small fossorial animals (toads, snakes, or rodents), whose burrows were observed in some units at the time of excavation (Figure 15). Burrows and micromorphological evidence of trampling suggest the possibility of time-averaging within the strata series. If the dissolution hypothesis presented above is generally correct, but the few bones remaining in the bone-poor zone are in good rather than bad condition, then these bones could represent recent material introduced into older layers via bioturbation in combination with gravity. The visibility and quantitative importance of these effects will be proportionately greatest in the units where the initially deposited bone was already lost by dissolution (Figure 16). The Aurignacian and Natufian lying above the Mousterian layer in Hayonim Cave would be a ready source of younger bone. New introductions would not have suffered the same fate as the Mousterian bones if the chemical environment had already stabilized. The lack of an empty stripe in the

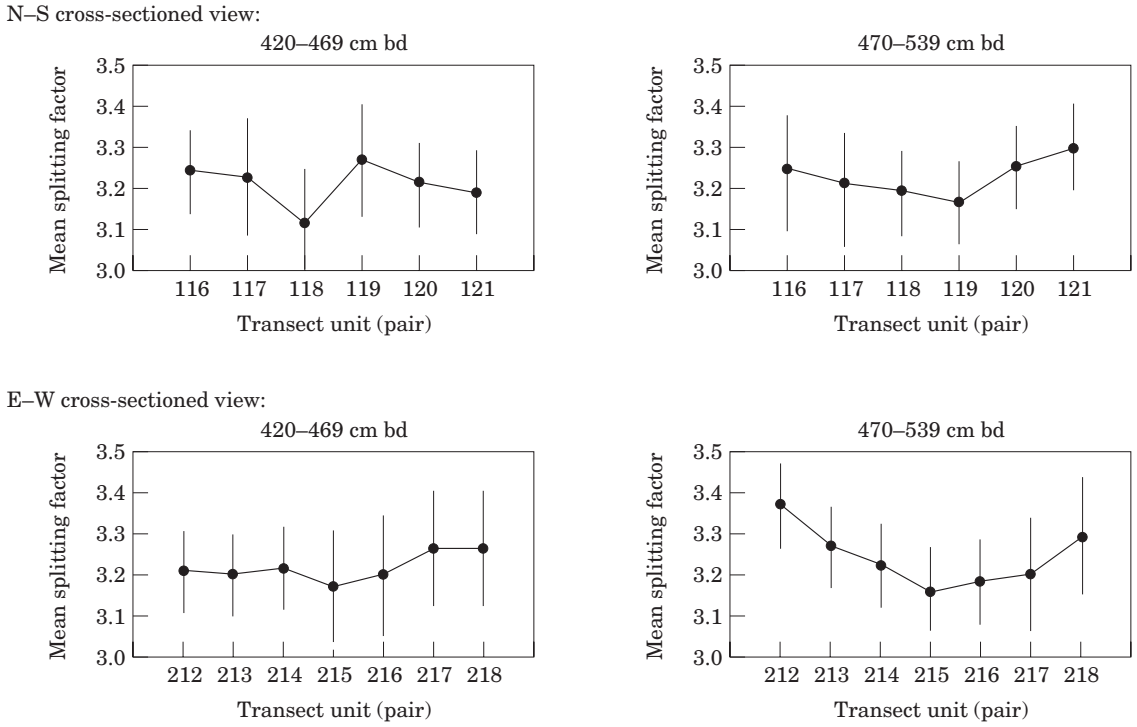


Figure 13. Mean splitting factor (SF) for FTIR-sampled bones from transect unit pairs, viewed N–S and E–W, above and below 470 cm bd. Vertical bars are standard deviations.

*Table 2. Infra-red splitting factor (SF) statistics for faunal specimens analysed (*N*) from transect unit pairs* in the Mousterian layer of the central trench, viewed N-S and E-W and organized by depth range*

| Excavation grid unit | Unit code | 420–469 cm bd | | | 470–539 cm bd | | |
|---|---|---|---|---|---|---|---|
| | | *N* | mean SF | S.D. | *N* | mean SF | S.D. |
| North–south view: | | | | | | | |
| I24a,c | 116 | 55 | 3·246 | 0·2 | 48 | 3·246 | 0·3 |
| I24b, I23d | 117 | 60 | 3·229 | 0·3 | 63 | 3·211 | 0·3 |
| J23a,c | 118 | 33 | 3·112 | 0·3 | 59 | 3·199 | 0·2 |
| J23b, J22d | 119 | 35 | 3·273 | 0·3 | 61 | 3·166 | 0·2 |
| K22a,c | 120 | 46 | 3·214 | 0·2 | 62 | 3·259 | 0·2 |
| K22b, K21d | 121 | 59 | 3·188 | 0·2 | 55 | 3·306 | 0·2 |
| East–west view: | | | | | | | |
| K21d | 212 | 33 | 3·201 | 0·2 | 29 | 3·370 | 0·2 |
| K22a,b | 213 | 49 | 3·200 | 0·2 | 55 | 3·271 | 0·2 |
| K22c, J22d | 214 | 39 | 3·222 | 0·2 | 60 | 3·226 | 0·2 |
| J23a,b | 215 | 41 | 3·168 | 0·3 | 58 | 3·160 | 0·2 |
| J23c, I23d | 216 | 44 | 3·200 | 0·3 | 62 | 3·185 | 0·2 |
| I24a,b | 217 | 51 | 3·266 | 0·3 | 54 | 3·204 | 0·3 |
| I24c | 218 | 25 | 3·265 | 0·3 | 30 | 3·300 | 0·3 |

*Adjacent units are paired to increase sample sizes in this comparison; paired unit codes correspond to x-axis labels in Figure 13.

distribution of Natufian or Aurignacian bones in layers D and B in the central trench confirms this.

## Scaling the Effects of Bioturbation

The great contrasts in bone preservation among units in the central trench can be used to gauge the extent of time-averaging in the Mousterian sediment series. Bioturbation's potential impact on the chronological integrity of the cultural strata is an important consideration, since the Mousterian layer is thick and is assumed to have resulted from a long occupation history. Attempts to scale the time-averaging effects of sediment disturbance are relatively new to

*Table 3. Representation of mineralized skeletal tissue classes* relative to bone abundance in the (a) central trench and (b) transect, based on large mammal, tortoise, and ostrich eggshell remains (NISP)*

| Mineralized tissue class | Percent by bone abundance zone: | | |
|---|---|---|---|
| | Bone-poor | Intermediate | Bone-rich |
| a. Central trench as a whole: | | | |
| sponge (e.g., horn core, antler, vertebrae) | 25 | 21 | 22 |
| fine sponge (e.g., carpals, tarsals, tortoise bone) | 41 | 48 | 48 |
| compact (e.g., mandible, long bones, phalanges) | 27 | 24 | 23 |
| stony (e.g., tooth enamel, ostrich eggshell) | 7 | 7 | 7 |
| total NISP: | (516) | (2112) | (9804) |
| b. Transect only: | | | |
| sponge (e.g., horn core, antler, vertebrae) | 14 | 23 | 22 |
| fine sponge (e.g., carpals, tarsals, tortoise bone) | 57 | 44 | 50 |
| compact (e.g., mandible, long bones, phalanges) | 22 | 22 | 22 |
| stony (e.g., tooth enamel, ostrich eggshell) | 7 | 11 | 6 |
| total NISP: | (113) | (436) | (3334) |

*Fresh bone is about 70% mineral, whereas mature tooth enamel (dahllite) and ostrich eggshell (calcite) are $\geq$95% mineral. Tissue codes, from least to most dense (following Wainwright *et al.*, 1976), are as follows:
(sponge)—Mostly spongy structure with thin compact bone covering. Macrostructure is relatively open, surface area to volume is relatively high, and thus this tissue class is the least dense of the four types named above.
(fine sponge)—Mostly a fine sponge structure with thin compact bone covering; these specimens naturally tend to be small. Surface area to volume is fairly high, but fine sponge tissue may resist diagenetic processes somewhat better than does open sponge tissue.
(compact)—Mostly compact or dense bone structure, but some spongy portions may also be present (e.g. epiphyses). Surface area to volume is comparatively low; tissue is relatively dense.
(stony)—Mostly or completely mineralized, highly crystalline structure with low surface to volume ratio; exceptionally dense and resistant to decomposition.
Note: Tissue categories are generalized; they ignore known heterogeneity in total element structure, because the question is about relative, surface-mediated differences in resistance to decomposition on an ordinal scale.

*Table 4. Fragmentation statistics for (a) all and (b) burned faunal specimens (NISP) from the bone-poor, intermediate, and bone-rich zones by depth range in the Mousterian layer, central trench*

| Bone abundance zone | 300–419 | | | 420–469 | | | 470–539 | | | All depths | | |
|---|---|---|---|---|---|---|---|---|---|---|---|---|
| | NISP | Mean | S.D. | NISP | Mean | S.D. | NISP | Mean | S.D. | NISP | Mean | S.D. |
| a. All specimens (burned and unburned): | | | | | | | | | | | | |
| Bone-poor | 61 | 3·7 | 2·0 | 132 | 3·1 | 1·7 | 124 | 2·7 | 1·4 | 351 | 3·1 | 1·7 |
| Intermediate | 160 | 3·6 | 1·7 | 265 | 3·2 | 2·0 | 1242 | 2·8 | 1·7 | 1698 | 3·0 | 1·8 |
| Bone-rich | 1199 | 3·5 | 2·1 | 6499 | 3·5 | 2·0 | 2635 | 2·7 | 1·6 | 10,367 | 3·3 | 2·0 |
| b. Burned specimens only: | | | | | | | | | | | | |
| Bone-poor | 11 | 3·0 | 1·1 | 15 | 2·5 | 1·5 | 25 | 2·4 | 1·1 | 59 | 2·6 | 1·2 |
| Intermediate | 31 | 3·0 | 1·8 | 36 | 2·5 | 1·5 | 293 | 2·2 | 1·0 | 366 | 2·4 | 1·2 |
| Bone-rich | 208 | 3·0 | 1·3 | 1119 | 3·0 | 1·7 | 479 | 2·2 | 1·3 | 1815 | 2·7 | 1·6 |

paleontology (see Flessa, Cutler & Meldahl, 1993; Kowalewski, Goodfriend & Flessa, 1998; Olszewski, 1999), and seldom is the approach taken to archaeological sites (but see Grave & Kealhofer, 1999). Scaling bioturbation effects may be most feasible in caves, because the inhabitable space tends to be limited, concentrating and superimposing cultural debris in relatively small areas. The probability that time-coherent sedimentary series will form in caves therefore is high, but, by virtue of the same conditions, the possibility for mixing younger and older material is also relatively great.

Downward migration of younger stone artifacts into layer E can be evaluated from the relative frequencies of post-Mousterian and Mousterian tool types. Time diagnostic artifacts generally make up a higher proportion of Epipaleolithic industries than is true for Mousterian industries, amplifying rather than suppressing signals of potential stratigraphic mixing in the case of Hayonim Cave. Table 6 shows that post-Mousterian artifacts constitute about 3% of all diagnostic tools in the upper section of the Mousterian layer (300–419 cm bd), about 2% in the middle section (420–469 cm bd), and 0% from the lowest section

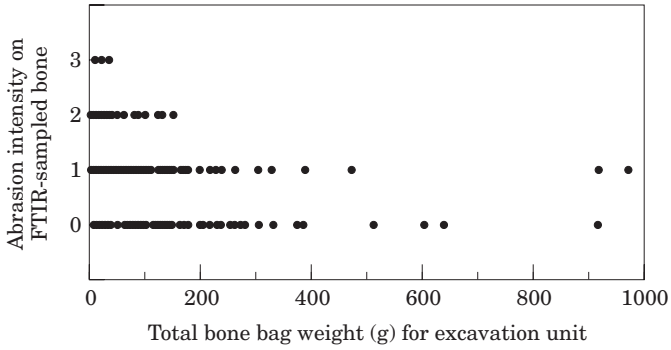


Figure 14. The intensity of abrasion damage on FTIR-sampled bone specimens relative to total screen-recovered bone bag weight (g) for the same excavation unit in the central trench.

(470–539 cm bd). Downward mixing could also have occurred in the lower sections of the Mousterian layer, but its aftermath can not be detected from the stone tools. The artifact proportions nonetheless indicate that (1) downward movement of younger material could be as high as 3% of the total assemblage, and (2) vertical migration usually occurred over short distances, since there is a clear decline in the frequency of post-Mousterian tools with depth.

It should be possible to evaluate whether bioturbation occurred in the deeper portion of the vertical Mousterian series of Hayonim Cave from the faunal remains, since the excavation units rich in bone flank those that are poor in bone throughout the sediment column. We assume that the initially deposited bones dissolved soon after burial, a scenario consistent with the proposal of Karkanas *et al.* (2000) for diagenesis rates in caves, and that all of the specimens in the bone-poor units could be intrusive. Table 7 compares the frequencies of identified bone (NISP) in the bone-rich and bone-poor units, subdivided into three vertical segments; bone-intermediate units are not considered. The contrasting bone frequencies indicate a potential addition of 2–5% (averaging 3% overall) of younger bone to the faunal assemblages of any vertical segment.

An average of 3% downward migration of bones (and presumably artifacts) is not a great deal of mixing, at least for layers that retain original bone in large quantities. Of course intrusive bones could constitute a high proportion of total bone where they penetrate units previously emptied of bone by dissolution. But intrusive bones constitute only a very minor proportion of the total bone in the dense Mousterian bone beds in Hayonim Cave. We conclude that the chronological integrity of the Hayonim cultural sequence in the central trench is essentially intact, but mild time-averaging occurred throughout the Mousterian series.

*Table 5. Inclination results for piece-plotted bones (*N*) from the Mousterian layer, central trench*

| Inclination range | *N* observed | % by bone abundance zone: | |
|---|---|---|---|
| | | Rich | Poor |
| Horizontal | 3040 | 86 | 75 |
| Inclined | 392 | 8 | 15 |
| Vertical | 262 | 6 | 9 |

Figure 15. Burrows cross-cutting Mousterian hearth lenses, damaging them but not destroying their visibility overall.

## Discussion and Conclusion

In Hayonim Cave calcite and dahllite are common in the Mousterian sedimentary units that also contain large quantities of bone. Decomposition products deriving from calcite and dahllite instead dominate the units in which bones are scarce. The macroscopic condition of preserved bones is very good, and only mild diagenetic activity (in the form of recrystallization) is indicated for the assemblages overall. The strong spatial agreement between the preservation conditions indicated by sediment mineralogy and bulk bone (and land snail shell) abundance points to dissolution as the primary cause of the patchy bone distributions. The hypothesis of an anthropogenic

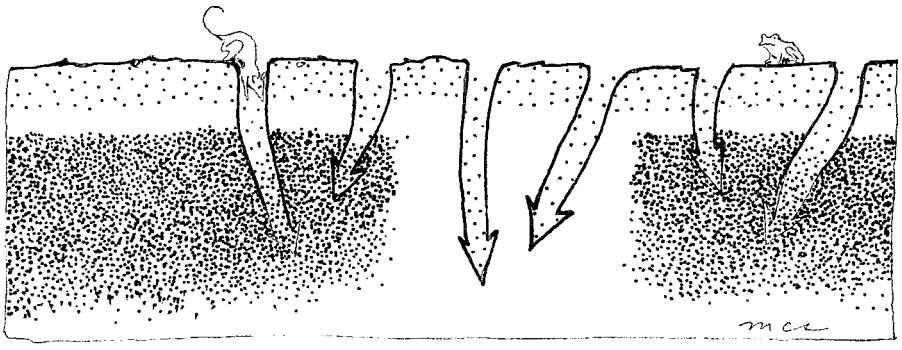

Figure 16. Scenario of the differential visibility of bioturbation effects in units preserving large quantities of original bone and units where original bone was lost by dissolution. Gravity tends to move younger material downward into older bone-rich and bone-depleted units as animals make and modify the burrows.

cause for these distributions in the central trench is refuted.

One might expect on the basis of these observations that the few bones recovered from the "bone-poor" units would be less well preserved on average. Contrary to expectation, bone mineral crystallinity (SF) and the ratio of fragile to resistant skeletal tissue types vary remarkably little across the bone-rich and bone-poor zones. The physical state of bone specimens is actually slightly better where bones are least abundant. Taken alone, the latter finding might seem to support the idea that heterogeneous bone distributions in the Middle Paleolithic layer resulted from variable disposal behaviours of prehistoric humans, habits that evidently did not apply to stone artifacts. However, the robust indications of preservation environment obtained from sediment mineralogy analysis prohibit this conclusion. The higher intensity of abrasion damage on bones from the bone-poor units along with the presence of younger, intrusive artifacts argue instead for a more complex story of faunal assemblage formation and preservation. The minor contradictions posed by bones within the dissolution zone add to the larger picture the likelihood of infrequent bioturbation.

Getting a grip on the issue of dissolution makes it possible to gauge the extent of stratigraphic mixing and, in so doing, evaluate the chronological integrity of the faunal series. Burrowing animals and penecontemporaneous trampling appear to have pulled younger materials downward in the sediments on occasion. This effect may appear greatest where sediments were decalcified. Small proportions of intrusive material indicate that bioturbation effects in the Mousterian layer of Hayonim Cave were relatively unimportant, at least in the many units where bone preservation is good. Bioturbation effects were proportionally great in units where bone preservation is poor, just metres away. Fortunately the total amount of well preserved bone in adjacent units nearly cancels out this effect in our case. A detailed view of these data nonetheless identifies the excavation areas that can yield faunal samples most suitable for paleoeconomic research.

To argue that differential skeletal body part representation or fragment refitting could resolve such questions about *in situ* loss at Hayonim Cave would be naïve. Some indicators of bone condition clearly disagree with those concerning sedimentary preservation environment, and are bound to mislead

*Table 6. Percentage of intrusive Epi- and Upper Paleolithic formal stone artifacts in the Mousterian layer by depth range, J-row of grid units only*

| | 300–419 cm bd | | | 420–469 cm bd | | | 470–539 cm bd | | |
|---|---|---|---|---|---|---|---|---|---|
| Square | pM | M | % pM† | pM | M | % pM† | pM | M | % pM* |
| J19 | 2 | 160 | 1·2 | 0 | 49 | 0 | 0 | 32 | 0 |
| J20 | 2 | 105 | 1·8 | 5 | 150 | 3·2 | 0 | 50 | 0 |
| J21 | 3 | 60 | 4·8 | 2 | 70 | 2·7 | 0 | 28 | 0 |
| J22 | 14 | 344 | 3·9 | 2 | 101 | 1·9 | 0 | 128 | 0 |
| J23 | 7 | 279 | 2·4 | 5 | 275 | 1·8 | 0 | 256 | 0 |
| J24 | 9 | 272 | 3·2 | 0 | 328 | 0 | 0 | 263 | 0 |
| all units | 37 | 1220 | 2·9 | 14 | 973 | 1·4 | 0 | 757 | 0 |

(pM) post-Mousterian artifacts; (M) Mousterian artifacts.
*The percentage (%) pM is calculated by dividing pM by the total number of diagnostic artifacts for all periods in a given spatial unit. Because later Paleolithic industries tend to contain higher proportions of time-diagnostic elements than do Mousterian industries, this analysis provides a *maximum estimate* of the contribution of younger intrusive material to the subject assemblage.

*Table 7. Percentage of inferred intrusive bone* through the Mousterian sediment column in the central trench, based on contrasting bone frequencies (NISP) in the bone-poor versus bone-rich units by depth range*

| Depth range (bd) | Bone-poor NISP | Bone-rich NISP | % Intrusive bone |
|---|---|---|---|
| 300–419 cm | 61 | 1199 | 5% |
| 420–469 cm | 132 | 6499 | 2% |
| 470–539 cm | 124 | 2635 | 5% |

*Percent intrusive bone is calculated as follows: first, bone-poor NISP is subtracted from bone-rich NISP; then bone-poor NISP is divided by "adjusted" bone-rich NISP. It is assumed for the sake of argument that all bones in the bone-poor units are intrusive, thus providing at maximum estimate. Units containing intermediate quantities of bone (g) are excluded from this comparison.

investigators if time-averaging effects are not also considered. It is likely that many other sites are characterized by these processes as well. We make this critical point while also providing some relatively cost-efficient means for solving the problem or assessing its severity.

The crisp boundaries between favourable and unfavourable preservation environments for calcite and dahllite—and thus for ash and bones—indicate the existence of dissolution fronts. Karkanas *et al.* (2000) probably are correct in their suggestion that most diagenesis occurs while buried material is close to the surface, and that, once started, phosphate and carbonate dissolution proceeds rapidly until a new chemical stability field (equilibrium) is reached. We sought evidence for transitional specimen states at the boundaries between bone-rich and bone-poor zones, following visible changes in sediment colour in the walls and floor of the excavation. While partly altered bone specimens exist in Hayonim Cave, they are exceedingly rare. It is in fact very difficult to detect "transitional" bone specimens, despite the obvious juxtaposition of favourable and unfavourable chemical environments in the cave sediments based on the mineralogy. The fact that there are similar proportions of downward migrating bones in the three segments of the Mousterian sediment column is consistent with the notion that the initially deposited bones dissolved soon after burial. The mineral decomposition processes seem to operate at the nanometer or molecular scale, and predictions of bone loss are not readily divisible at the scale of bone macrostructure (e.g., compact versus spongy bone).

Changes in mineral composition in Hayonim therefore appear to have been rapid and thorough while the chemical conditions were reactive. All-or-nothing preservation situations may prevail in Hayonim Cave, and probably in other sites as well. The problems of preservation and phosphate diagenesis seem to be especially acute in Mediterranean caves, and are perhaps somewhat less severe in colder areas of Europe. Additionally, we find no consistent relation between infra-red data on a vertical gradient and the age of the cultural material in our sample, nor between the Mousterian, Kebaran, and Natufian layers. These data are in general agreement with Sillen's (1981) earlier findings on calcium/phosphate ratios for Natufian and Aurignacian samples from Hayonim Cave. The results, however, argue against the general possibility of using levels of apatite recrystallization for relative dating purposes (Sillen & Parkington, 1996).

It is crucial to identify past and current chemical environments in a site, molecular traces of which often are preserved in sediments despite the loss of visible bone and hearth features. Combining macroscopic and FTIR observations provides a more comprehensive picture of the taphonomic history of faunal remains in Hayonim Cave, a relatively complex situation that is to some degree typical of Mediterranean and other mid-latitude limestone caves. Identifying "preservation zones" in sites greatly simplifies a host of other assumptions about the quality of faunal data for paleoeconomic studies and may prove more effective and economical than approaches such as comprehensive refitting of specimens.

## Acknowledgements

We thank the Israel Antiquities Authority for permission to export faunal samples from Hayonim Cave to the University of Arizona (U.S.A.) for the FTIR and fragmentation analyses. We are indebted to P. J. Brantingham, X. Gao, A. Margaris, L. Bergstresser, N. Munro, R. Shahack, and A. Stutz for their assistance to this study in the laboratory and/or the field; and to E. Tchernov, M. Tite, and M. Sponheimer for general comments. Thanks also to R. Lee Lyman and one anonymous *JAS* reviewer for thoughtful criticisms and comments. This research is supported by a NSF CAREER grant to Stiner (SBR-9511894), an Israel Science Foundation grant to Weiner, and a NSF grant to Bar-Yosef (SBR-9409281).

## References

Albert, R. M., Lavi, O., Estroff, L., Weiner, S., Tsatskin, A., Ronen, A. & Lev-Yadun, S. (1999). Occupation of Tabun Cave, Mt. Carmel, Israel, during the Mousterian period: a study of the sediments and phytoliths. *Journal of Archaeological Science* **26,** 1249–1260.

Bar-Yosef, O. (1991). The archaeology of the Natufian layer at Hayonim Cave. In (O. Bar-Yosef & F. Valla, Eds) *The Natufian Culture in the Levant*. Ann Arbor, MI: International Monographs in Prehistory, pp. 81–93.

Bar-Yosef, O. (1998). The chronology of the Middle Paleolithic of the Levant. In (T. Akazawa, K. Aoki & O. Bar-Yosef, Eds) *Neanderthals and Modern Humans in West Asia*. New York: Plenum Press, pp. 39–56.

Bar-Yosef, O., Vandermeersch, B., Arensburg, B., Belfer-Cohen, A., Goldberg, P., Laville, H., Meignen, L., Rak, Y., Speth, J. D., Tchernov, E., Tillier, A.-M. & Weiner, S. (1992). The excavations in Kebara Cave, Mt. Carmel. *Current Anthropology* **33,** 497–550.

Belfer-Cohen, A. & Bar-Yosef, O. (1981). The Aurignacian at Hayonim Cave. *Paleorient* **7,** 19–42.

Berner, R. A. (1971). *Principles of Chemical Sedimentology*. New York: McGraw Hill.

Featherstone, J. D. B., Pearson, S. & LeGeros, R. Z. (1984). An infrared method for quantification of carbonate in carbonated apatites. *Caries Research* **18,** 63–66.

Flessa, K. W., Cutler, A. H. & Meldahl, K. H. (1993). Time and taphonomy: quantitative estimates of time-averaging and stratigraphic disorder in a shallow marine habitat. *Paleobiology* **19,** 266–286.

Goldberg, P. & Bar-Yosef, O. (1998). Site formation processes in Kebara and Hayonim Caves and their significance in Levantine prehistoric caves. In (T. Akazawa, K. Aoki & O. Bar-Yosef, Eds) *Neanderthals and Modern Humans in West Asia*. New York: Plenum Press, pp. 107–125.

Grave, P. & Kealhofer, L. (1999). Assessing bioturbation in archaeological sediments using soil morphology and phytolith analysis. *Journal of Archaeological Science* **26,** 1239–1248.

Hedges, R. E. M. & Millard, A. (1995). Bones and groundwater: towards the modelling of diagenetic processes. *Journal of Archaeological Science* **22,** 155–164.

Hedges, R. E. M., Millard, A. & Pike, A. W. G. (1995). Measurements and relationships of diagenetic alteration of bone from three archaeological sites. *Journal of Archaeological Science* **22,** 201–209.

Humphreys, G. S., Hunt, P. & Buchanan, R. (1987). Wood-ash stone near Sydney, N.S.W.: a carbonate pedological feature in an acidic soil. *Australian Journal of Soil Research* **25,** 115–124.

Karkanas, P., Kyparissi-Apostolika, N., Bar-Yosef, O. & Weiner, S. (1999). Mineral assemblages in Theopetra, Greece: a framework for understanding diagenesis in a prehistoric cave. *Journal of Archaeological Science* **26,** 1171–1180.

Karkanas, P., Bar-Yosef, O., Goldberg, P. & Weiner, S. (2000). Diagenesis in prehistoric caves: the use of minerals that form in situ to assess the completeness of the archaeological record. *Journal of Archaeological Science* in press.

Kowalewski, M., Goodfriend, G. A. & Flessa, K. W. (1998). High-resolution estimates of temporal mixing within shell beds: the evils and virtues of time-averaging. *Paleobiology* **24,** 287–304.

McConnell, D. (1952). The crystal chemistry of carbonate apatites and their relationship to the composition of calcified tissues. *Journal Dental Research* **31,** 53–63.

Meignen, L., Bar-Yosef, O. & Goldberg, P. (1989). Les structures de combustion moustériennes de la grotte de Kébara (Mont Carmel, Israël). *Actes du Colloque de Nemours 1987, Mémoires du Musée de Préhistoire d'Ile de France*, no. 2, pp. 141–146.

Olszewski, T. (1999). Taking advantage of time averaging. *Paleobiology* **25,** 226–238.

Person, A., Bocherens, H., Mariotti, A. & Renard, M. (1996). Diagenetic evolution and experimental heating of bone phosphate. *Palaeogeography, Palaeoclimatology and Palaeoecology* **126,** 135–149.

Robinson, R. A. (1952). An electron microscope study of the crystalline inorganic components of bone and its relationship to the organic matrix. *Journal of Bone Joint Surgery* **34A,** 389–434.

Schiegl, S., Lev-Yadun, S., Bar-Yosef, O., El Goresy, A. & Weiner, S. (1994). Siliceous aggregates from prehistoric wood ash: a major component of sediments in Kebara and Hayonim Caves (Israel). *Israel Journal of Earth Sciences* **43,** 267–278.

Schiegl, S., Goldberg, P., Bar-Yosef, O. & Weiner, S. (1996). Ash deposits in Hayonim and Kebara Caves, Israel: macroscopic, microscopic and mineralogical observations, and their archaeological implications. *Journal of Archaeological Science* **23,** 763–781.

Schwarcz, H. P. & Rink, W. J. (1998). Progress in ESR and U-Series chronology of the Levantine Paleolithic. In (T. Akazawa, K. Aoki & O. Bar-Yosef, Eds) *Neanderthals and Modern Humans in West Asia*. New York: Plenum Press, pp. 57–67.

Shipman, P., Foster, G. F. & Schoeninger, M. (1984). Burnt bones and teeth: an experimental study of colour, morphology, crystal structure and shrinkage. *Journal of Archaeological Science* **11,** 307–325.

Sillen, A. (1981). Post-depositional changes in Natufian and Aurignacian faunal bones from Hayonim Cave. *Paléorient* **7,** 81–85.

Sillen, A. & Parkington, J. (1996). Diagenesis of bones from Eland's Bay Cave. *Journal of Archaeological Science* **23,** 535–542.

Smith, B. C. (1996). *Fundamentals of Fourier Transform Infrared Spectroscopy*. Boca Raton: CRC Press.

Stiner, M. C. & Tchernov, E. (1998). Pleistocene species trends at Hayonim Cave: Changes in climate versus human behavior. In (T. Akazawa, K. Aoki & O. Bar-Yosef, Eds) *Neanderthals and Modern Humans in West Asia*. New York: Plenum Press, pp. 241–262.

Stiner, M. C., Weiner, S., Bar-Yosef, O. & Kuhn, S. L. (1995). Differential burning, fragmentation, and preservation of archaeological bone. *Journal of Archaeological Science* **22,** 223–237.

Surovell, T. A. & Stiner, M. C. (2001). Standardization of infrared measures of bone mineral crystallinity: an experimental approach. *Journal of Archaeological Science* **28,** 633–642.

Tchernov, E. (1994). New comments on the biostratigraphy of the Middle and Upper Pleistocene of the southern Levant. In (O. Bar-Yosef & R. S. Kra, Eds) *Late Quaternary Chronology and Paleoclimates of the Eastern Mediterranean*. RADIOCARBON, pp 333–350.

Tchernov, E. (1998). The faunal sequence of the southeast Asian Middle Paleolithic in relation to hominid dispersal events. In (T. Akazawa, K. Aoki & O. Bar-Yosef, Eds) *Neanderthals and Modern Humans in West Asia*. New York: Plenum Press, pp. 77–90.

Termine, J. D. & Posner, A. S. (1966). Infrared analysis of rat bone: age dependency of amorphous and crystalline mineral fractions. *Science* **153,** 1523–1525.

Valladas, H., Mercier, N., Joron, J.-L. & Reyss, J.-L. (1998). GIF Laboratory dates for Middle Paleolithic Levant. In (T. Akazawa, K. Aoki & O. Bar-Yosef, Eds) *Neanderthals and Modern Humans in West Asia*. New York: Plenum Press, pp. 69–75.

Wainwright, S. A., Briggs, W. D., Currey, J. D. & Gosline, J. M. (1976). *Mechanical Design in Organisms*. Princeton: Princeton University Press.

Weiner, S. & Bar-Yosef, O. (1990). States of preservation of bones from prehistoric sites in the Near East: a survey. *Journal of Archaeological Science* **17,** 187–196.

Weiner, S. & Goldberg, P. (1990). On-site Fourier Transform Infrared Spectrometry at an archaeological excavation. *Spectroscopy* **5,** 46–50.

Weiner, S., Goldberg, P. & Bar-Yosef, O. (1993). Bone preservation in Kebara Cave, Israel, using on-site Fourier transform infra-red spectrometry. *Journal of Archaeological Science* **20,** 613–627.

Weiner, S., Schiegl, S., Goldberg, P. & Bar-Yosef, O. (1995). Mineral assemblages in Kebara and Hayonim caves, Israel: excavation strategies, bone preservation, and wood ash remnants. *Israel Journal of Chemistry* **35,** 143–154.

Weiner, S. & Traub, W. (1992). Bone structure: from ångstroms to microns. *The FASEB Journal* **6,** 879–885.

Weiner, S. & Price, P. A. (1986). Disaggregation of bone into crystals. *Calcified Tissue Research* **39,** 365–375.

Wright, L. E. & Schwarcz, H. P. (1996). Infra-red and isotopic evidence for diagenesis of bone apatite at Dos Pilas, Guatemala: paleodietary implications. *Journal of Archaeological Science* **23,** 933–944.

Ziv, V. & Weiner, S. (1994). Bone crystal sizes: a comparison of transmission electron microscope and X-ray diffractions in width broadening techniques. *Connective Tissue Research* **30,** 165–175.